





## Article

# Synthesis, Characterization and Photodegradation Studies of Copper Oxide–Graphene Nanocomposites

Indah Raya <sup>1</sup>, Awais Ahmad <sup>2</sup>, Ayad F. Alkaim <sup>3</sup>, Dmitry Bokov <sup>4</sup>, Enas R. Alwaily <sup>5</sup>, Rafael Luque <sup>2,\*</sup>, Mabkhoot Alsaiani <sup>6,7,\*</sup> and Mohammed Jalalah <sup>6,8</sup>

- <sup>1</sup> Department of Chemistry, Faculty Mathematics and Natural Science, Hasanuddin University, Makassar 90245, Indonesia; indahraya@unhas.ac.id
  - <sup>2</sup> Departamento de Química Organica, Universidad de Cordoba, Edificio Marie Curie (C-3), Ctra Nnal IV-A, Km 396, E14014 Cordoba, Spain; awaisahmed@gcuf.edu.pk
  - <sup>3</sup> Department of Chemistry, College of Science for Women, University of Babylon, Hilla 51002, Iraq; alkaimayad@gmail.com
  - <sup>4</sup> Institute of Pharmacy, Sechenov First Moscow State Medical University, 119991 Moscow, Russia; fmmsu@mail.ru
  - <sup>5</sup> Microbiology Research Group, College of Pharmacy, Al-Ayen University, Nasiriyah 64011, Iraq; Enas.kazem@alayen.edu.iq
  - <sup>6</sup> Promising Centre for Sensors and Electronic Devices (PCSED), Advanced Materials and Nano-Research Centre, Najran University, Najran 11001, Saudi Arabia; jalalah@gmail.com
  - <sup>7</sup> Empty Quarter Research Unit, Department of Chemistry, College of Science and Art in Sharurah, Najran University, Najran 11001, Saudi Arabia
  - <sup>8</sup> Department of Electrical Engineering, College of Engineering, Najran University, Najran 11001, Saudi Arabia
- \* Correspondence: q62alsor@uco.es (R.L.); mabkhoot.alsaiani@gmail.com (M.A.)



**Citation:** Raya, I.; Ahmad, A.; Alkaim, A.F.; Bokov, D.; Alwaily, E.R.; Luque, R.; Alsaiani, M.; Jalalah, M. Synthesis, Characterization and Photodegradation Studies of Copper Oxide–Graphene Nanocomposites. *Coatings* **2021**, *11*, 1452. <https://doi.org/10.3390/coatings11121452>

Academic Editor: Teen-Hang Meen

Received: 19 October 2021

Accepted: 19 November 2021

Published: 26 November 2021

**Publisher's Note:** MDPI stays neutral with regard to jurisdictional claims in published maps and institutional affiliations.



**Copyright:** © 2021 by the authors. Licensee MDPI, Basel, Switzerland. This article is an open access article distributed under the terms and conditions of the Creative Commons Attribution (CC BY) license (<https://creativecommons.org/licenses/by/4.0/>).

**Abstract:** In this work, a simple hydrothermal method was employed to prepare a pristine sample of copper oxide (CuO) and three samples of copper oxide–graphene nanocomposites (CuO-xG) with  $x = 2.5, 5,$  and  $10$  mg of graphene. The synthesized samples were characterized using X-ray powder diffractometry (XRD), field emission scanning electron microscopy (FESEM), energy-dispersive X-ray spectroscopy (EDX), Fourier-transform infrared spectroscopy (FTIR) and ultraviolet–visible (UV-Vis) spectroscopy. The XRD patterns of CuO-xG nanocomposites exhibited the diffraction peaks related to the crystal planes of monoclinic CuO and hexagonal graphite. The surface morphology of the prepared samples was investigated using FESEM images. EDX analysis was used to investigate the chemical composition of the synthesized samples. FTIR spectroscopy identified the vibrational modes of the covalent bonds present in the samples. The allowed direct optical bandgap energy was calculated for all prepared samples using UV-Vis absorption spectra. The small bandgap of CuO-xG nanocomposites indicates their potential use as an effective photocatalyst in the presence of visible light. Photocatalytic activity of the samples was explored for the degradation of methylene blue (MB) dye contaminant under visible light irradiation. The results showed that the CuO-5G sample has the highest photodegradation efficiency (~56%).

**Keywords:** CuO–graphene nanocomposite; hydrothermal synthesis; structural properties; FESEM; optical bandgap; photocatalytic activity

## 1. Introduction

In recent years, hybrid graphene nanocomposites have been of great research interest due to their potential use in different technological applications [1–5]. To meet the specific requirements of various industrial applications, there has been an ever-increasing need for the development of novel functional materials with more favorable features [6–10].

Due to their special properties such as cost-effective fabrication procedure, good chemical stability, eco-friendliness, high theoretical specific capacity, and abundant availability, transition metal oxides (TMOs) including  $\text{Fe}_2\text{O}_3$ ,  $\text{Co}_3\text{O}_4$ , NiO and CuO have at-

tracted considerable attention for use in various applications, including solar cells, photocatalysts, electrode materials, and gas sensors [11–17]. However, TMOs have some drawbacks such as low conductivity, pulverization, and aggregation caused by large volume expansion [18–20]. These drawbacks lead to fast capacity attenuation during the charge/discharge process and therefore limit TMOs practical applications [21–25].

CuO is a p-type semiconductor with a bandgap of  $\sim 1.2$  eV in its bulk form [26]. CuO has been successfully used in solar cells [27,28], sensors [29,30], batteries [31,32], biosensing [33], water remediation [33,34], CO<sub>2</sub> conversion [7], and heterogeneous catalysis for degradation of several dyes [35–37]. Owing to its narrow bandgap, CuO can be considered as a proper alternative to other wide bandgap semiconducting nanomaterials. It should be noted that the narrow bandgap of copper oxide causes very fast electron-hole recombination, which limits the photocatalytic activity [38].

Carbonaceous nanomaterials like mesoporous carbon, carbon nanotubes and carbon nanofibers have demonstrated good performance as catalyst support materials for different applications [39–42]. Graphene, as the fundamental building block of all graphitic materials, is composed of a single layer of sp<sup>2</sup> bonded carbon atoms [43,44]. Chemical inertness, unraveled electrical properties, high mechanical strength, good thermal conductivity and ultrahigh surface area are some of the extraordinary properties [45] that make graphene a promising material for many applications such as field-effect transistors [46], batteries [47,48], fuel cells [49], solar cells [50], supercapacitors [51], and biosensors [52]. For use in the practical graphene/metal composites, the poor dispersion of graphene in metal matrix and weak graphene/metal interfacial bonding are considered as two main drawbacks. Interfacial interaction between a metal oxide and graphene gives us the ability to control the morphology and size of inorganic particles grown on the surface of graphene nanosheets (GNSs) [53–57]. This interaction influences the charge transport and rate performance as well as the ability to withstand repeating lithiation/delithiation of electrode materials [58].

Copper matrix composite reinforced with graphene has recently attracted much attention. Introducing graphene into the copper matrix, effectively improves the electrical, thermal, and electrical properties of the composites [59,60]. However, due to the aggregation of graphene in the Cu matrix, the mechanical properties of the graphene/Cu composites are still unsatisfying. This gives rise to the importance of the synthesis of Cu-matrix composite with uniformly dispersed graphene. In this regard, graphene-induced bandgap widening and luminescence quenching in ceria-graphene composites has been reported elsewhere [61–63]. Additionally, the loading of graphene increased the absorption and photocatalytic activity of the Fe<sub>2</sub>O<sub>3</sub> in the Fe<sub>2</sub>O<sub>3</sub>/rGO composites [64–67]. Compared to CuO nanostructures, the nanocomposites formed by immobilization of CuO nanostructures on graphene-based materials have a completely distinct performance [68–70]. In addition to having a combination of individual features of constituents, functionalization or interaction or charge transfer between graphene and CuO nanostructures can introduce new features in the CuO nanostructures.

To overcome the limitations of copper oxide applications, its chemical structure must be improved. Incorporating CuO with graphene might be a suitable candidate for doing this improvement since graphene reduces the rate of electron-hole recombination [38]. Graphene, as a perfect absorber of light [71], can also supply the electrons required for photocatalytic reactions. The present work has been performed to experimentally investigate the structural, morphological, compositional, optical and photodegradation properties of newly synthesized CuO-graphene nanocomposites.

## 2. Materials and Methods

### 2.1. Materials

Copper (II) acetate, Cetyl trimethyl ammonium bromide (CTAB), sodium hydroxide, ethanol, multilayer graphene and methylene blue were used as starting materials. Table 1 represents some information on these chemicals.

**Table 1.** Chemical information of starting materials.

Component	Chemical Formula	CAS Number	Molar Mass (g/mol)	Supplier	Purity
Copper (II) Acetate	Cu (CH <sub>3</sub> COO) <sub>2</sub>	6046-93-1	199.65	Merck	99.99%
Cetyl trimethyl ammonium bromide	C <sub>19</sub> H <sub>42</sub> BrN	57-09-0	364.45	Merck	99.99%
Sodium hydroxide	NaOH	1310-73-2	40	Merck	99.99%
Ethanol	C <sub>2</sub> H <sub>5</sub> OH	64-17-5	46.07	Merck	99.99%
Methylene blue	C <sub>16</sub> H <sub>18</sub> ClN <sub>3</sub> S	61-73-4	319.85	Sigma-Aldrich	95%
Graphene	C	1034343-98-0	12.01	US Research Nanomaterials, Inc.	95%

## 2.2. Synthesis

CuO-xG nanocomposites with x = 2.5, 5 and 10 mg of graphene were synthesized using a simple hydrothermal method. In the first step, 2.5 mg of graphene was poured into a breaker containing 25 mL of 50:50 % ethanol-water solution. The obtained mixture was dispersed by ultrasonication for 15 min. The beaker was then placed on a magnetic stirrer and 0.11 g of copper acetate was added to the mixture while stirring. After 10 min, 0.3 g of CTAB was also added to the mixture. In the next step, 0.04 g of sodium hydroxide was added to 20 mL of another 50:50 % ethanol-water solution and after mixing for a while, it was added drop by drop to the original mixture. After approximately 10 min, the color of the mixture turned dark green. After 45 min, when the precursors were well mixed, the obtained mixture was poured into a 50 mL Teflon container and placed in an autoclave. The autoclave was then completely sealed and placed in a chamber furnace for 12 h at 135 °C. The synthesized material was then removed from the autoclave and washed several times by centrifugation at 6000 rpm for 5 min. The sample was then transferred to an incubator to dry at 60 °C for 12 h. This sample was named CuO-2.5G. To assess the effect of graphene addition on the structural, optical and photocatalytic properties of CuO, a pristine CuO sample as well as two other copper oxide-graphene nanocomposites (CuO-5G and CuO-10G) were prepared by the same method.

## 2.3. Sample Characterizations

To study the structural phases of the synthesized samples, XRD patterns of all synthesized samples were obtained in powdered form at room temperature by a Panalytical PW1730 diffractometer (JDX-3532, JEOL, Tokyo, Japan) using Cu K<sub>α</sub>1 radiation ( $\lambda = 1.540598 \text{ \AA}$ ) with a scanning angle ( $2\theta$ ) varied from 20° to 80° and scanning step width of 0.02. The XRD profiles were analyzed by ANalytical X'Pert HighScore software and compared to standards compiled by the Joint Committee on Powder Diffraction and Standards (JCPDS). Investigation of the surface morphology of the samples and their elemental analysis were performed using a MIRA3-TESCAN FESEM Sigma, Zeiss, Jena, Germany) equipped with an EDX system. Suspension of nanomaterials was performed in ethanol and drop cast on glass slides. These samples were stuck on carbon tape after drying and then subjected to carbon coating. FTIR spectra of CuO and all synthesized nanocomposites inserted in KBr powder system are investigated in the frequency range of 400–4000 cm<sup>-1</sup> using a BFRL Rayleigh FTIR WQF-510 spectrometer (Perkin Elmer) (IR Prestige21, Shimadzu, Kyoto, Japan). The UV-Visible absorption spectra were also recorded at room temperature using a Shimadzu UV-1800 UV-VIS spectrophotometer (Shimadzu-2700 spectrophotometer) equipped with an integrating sphere, in which white BaSO<sub>4</sub> was served as the reference material in the wavelength region of 200–1000 nm.

## 2.4. Photocatalytic Activity of the Samples

Photocatalytic experiments were carried out at room temperature (24 °C) by photodegrading MB dye with a 100 W household light bulb. To do so, 20 mg of each synthesized sample was added separately into 50 mL of 100 ppm MB solution. Before illumination, the suspensions were continuously stirred at a dark place at room temperature for 30 min to reach an adsorption-desorption equilibrium. Then, the suspensions were exposed to

visible light irradiation for 9 h at room temperature. At regular 1-h intervals, 5 cc (cubic centimeter) samples were taken from the suspensions and analyzed using a Shimadzu UV-1800 UV-VIS spectrophotometer in the wavelength region of 300–1100 nm.

### 3. Results

#### 3.1. Structural and Morphological Analysis

Figure 1 illustrates the XRD patterns of the as-prepared pristine CuO and CuO-xG (x = 2.5, 5 and 10 mg of graphene) samples. The diffraction peaks and their corresponding crystal planes are listed in Table 2. All the peaks obtained for the pristine CuO sample can be attributed to the monoclinic phase of CuO (space group C2/c;  $a_0 = 4.685 \text{ \AA}$ ,  $b_0 = 3.423 \text{ \AA}$ ,  $c_0 = 5.132 \text{ \AA}$  and  $\beta = 99.47^\circ$ ; JCPDS Card no. 48-1548) [72]. The peak obtained at  $2\theta = 26.67^\circ$  for the CuO-2.5G and CuO-5G samples is the signature of (002) plane of the hexagonal graphite structure, suggesting that the graphene is incorporated with the CuO. The other peaks in the XRD profiles of CuO-2.5G and CuO-5G nanocomposites are assigned to the monoclinic phase of CuO. The XRD profile of CuO-10G sample exhibits a diffraction peak at  $2\theta = 26.67^\circ$  corresponding to (002) plane of the hexagonal graphite structure, as well as two peaks at  $2\theta = 32.47^\circ$  and  $2\theta = 35.61^\circ$  related to the ( $\bar{1}11$ ) and (111) planes of the monoclinic phase of CuO. The average crystallite sizes of graphene and CuO were calculated for all samples using the Debye–Scherrer equation [73].

$$D = k\lambda / \beta \cos\theta \quad (1)$$

where  $k$  is a constant which equals 0.9,  $\lambda$  is the wavelength of the X-ray radiation ( $\lambda = 1.540598 \text{ \AA}$ ),  $\beta$  is the corrected band broadening (full-width at half-maximum (FWHM)) after subtraction the equipment broadening, and  $\theta$  is the Bragg angle. In these calculations, the peak corresponding to the (002) plane was used for graphene, and the peak linked to the ( $\bar{1}11$ ) plane was considered for CuO. The values obtained for the average crystallite sizes are given in Table 3. As is clear, the average crystallite size of CuO increases from 8.46 to 10.32 nm with the addition of 2.5 mg graphene, but it falls slightly to 10.19 nm when the amount of graphene in the nanocomposite reaches 5 mg. Furthermore, when 10 mg graphene is combined with copper oxide, the average crystallite size of CuO grows to 12.47 nm. From Table 3, the average crystallite size of graphene increases as the amount of graphene incorporated with CuO increases.

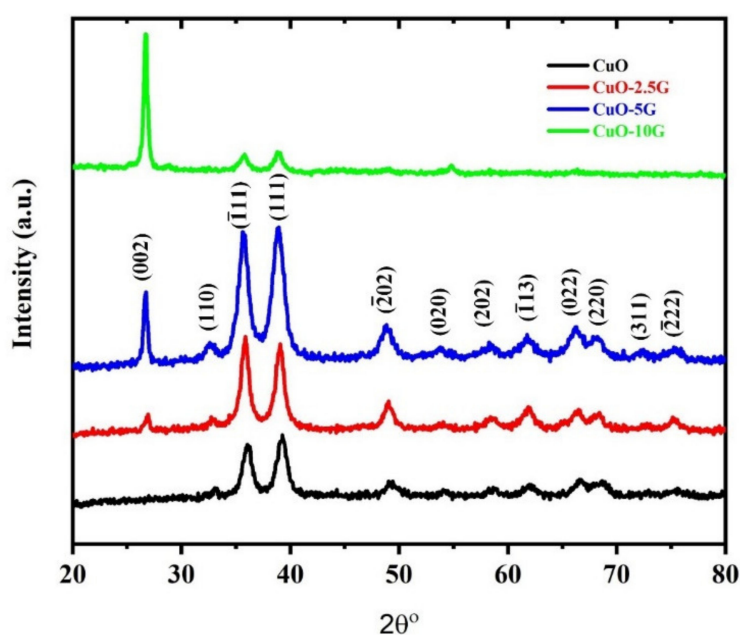


Figure 1. XRD patterns of pristine CuO, CuO-2.5G, CuO-5G and CuO-10G nanocomposites.

**Table 2.** X-ray diffraction peaks of the prepared samples and their associated crystal planes.

Sample							
CuO		CuO-2.5G		CuO-5G		CuO-10	
2 $\theta$	Plane	2 $\theta$	Plane	2 $\theta$	Plane	2 $\theta$	Plane
32.47	110	26.67	002	26.67	002	26.67	002
35.61	$\bar{1}11$	32.47	001	32.47	001	32.47	$\bar{1}11$
35.82	111	35.61	$\bar{1}11$	35.61	$\bar{1}11$	35.61	111
49.04	$\bar{2}02$	35.82	$\bar{2}02$	35.82	$\bar{2}02$	-	-
58.51	202	38.85	020	38.85	020	-	-
61.79	$\bar{1}13$	49.04	202	49.04	202	-	-
66.22	022	53.72	$\bar{1}13$	53.72	$\bar{1}13$	-	-
68.27	220	58.51	022	58.51	022	-	-
—	—	61.79	220	61.79	220	-	-
—	—	66.22	311	66.22	311	-	-
—	—	68.27	$\bar{2}22$	68.27	$\bar{2}22$	-	-

**Table 3.** Calculated average crystallite sizes of CuO and graphene in the synthesized samples.

Sample	Average Crystallite Size	
	CuO	Graphene
CuO	8.46	0.00
CuO-2.5G	10.32	15.40
CuO-5G	10.19	20.98
CuO-10G	12.47	26.02

The FESEM images of the pristine CuO sample and the CuO-2.5G, CuO-5G and CuO-10G nanocomposites are represented in Figure 2a,b and Figure 3a,b, respectively. Figure 2a shows a grain structure for the pristine CuO sample with an average grain diameter of around 31.95 nm. When CuO is incorporated with graphene, we see the formation of graphene sheets on which CuO grains appear to grow. The presence of the sheets becomes clearer with increasing the amount of graphene in the nanocomposite. The average diameter of grains grown on the graphene sheets is about 28.92, 20.11 and 40.85 nm for CuO-2.5G, CuO-5G and CuO-10G nanocomposites, respectively (see Table 4). When the amount of graphene is low, ultrasonic dispersion can cause the graphene to disperse well. However, when the amount of addition is large (~10 mg), the graphene is not easily dispersed, and agglomerates obviously.

EDX analysis was used to investigate the chemical composition of the synthesized samples. The obtained EDX spectra are shown in Figure 4. The weight and atomic percentages of the elements found in the samples are also provided in Table 5. The EDX spectrum of pristine CuO (see Figure 4a) confirms the presence of Cu and O elements in this sample. Additionally, the EDX spectra of CuO-xG nanocomposites (x = 2.5, 5 and 10 mg of graphene) indicate the presence of three main elements including Cu, O and C, further demonstrating the successful formation of the samples. The EDX spectra present the high content of oxygen in the nanocomposites which could be predicted due to formation of graphene oxide [74], which are further confirmed by the C=O and C–O vibrational peaks in FTIR spectra.

### 3.2. FTIR Spectroscopy Analysis

FTIR spectroscopy provides significant information on the molecular vibrations and rotations associated with different covalent bonds found in the chemical compositions. The FTIR spectra of CuO-xG (x = 2.5, 5 and 10 mg) nanocomposites are represented in Figure 5. The assignments of the observed absorption peaks are also provided in Table 6. The presence of the typical absorption peaks of Cu–O bond (around 506 and 593  $\text{cm}^{-1}$ ) confirms the formation of CuO structure in the nanocomposites. Additionally, the peaks



related to C=O and C-O bonds verify the existence of graphene in the synthesized samples. The peaks assigned to C-H and O-H bonds might be due to impurities in the samples. As expected, by increasing the amount of graphene from 2.5 to 5 mg, three new absorption peaks appeared in the FTIR spectrum of CuO-5G nanocomposite (at around 728, 910 and 960  $\text{cm}^{-1}$ ). These additional peaks are related to the vibration modes of C=O bond. Additionally, by further increasing of graphene amount from 5 to 10 mg, two other new peaks are detected in the spectrum of CuO-10G (at  $\sim 804$  and  $\sim 1022$   $\text{cm}^{-1}$ ), which are linked to C-C and C-O-C bonds, respectively.

**Table 4.** The average grain diameter of pristine CuO, CuO-2.5G, CuO-5G and CuO-10G nanocomposites.

Sample	Average Grain Diameter
CuO	31.95
CuO-2.5G	28.92
CuO-5G	20.11
CuO-10G	40.85

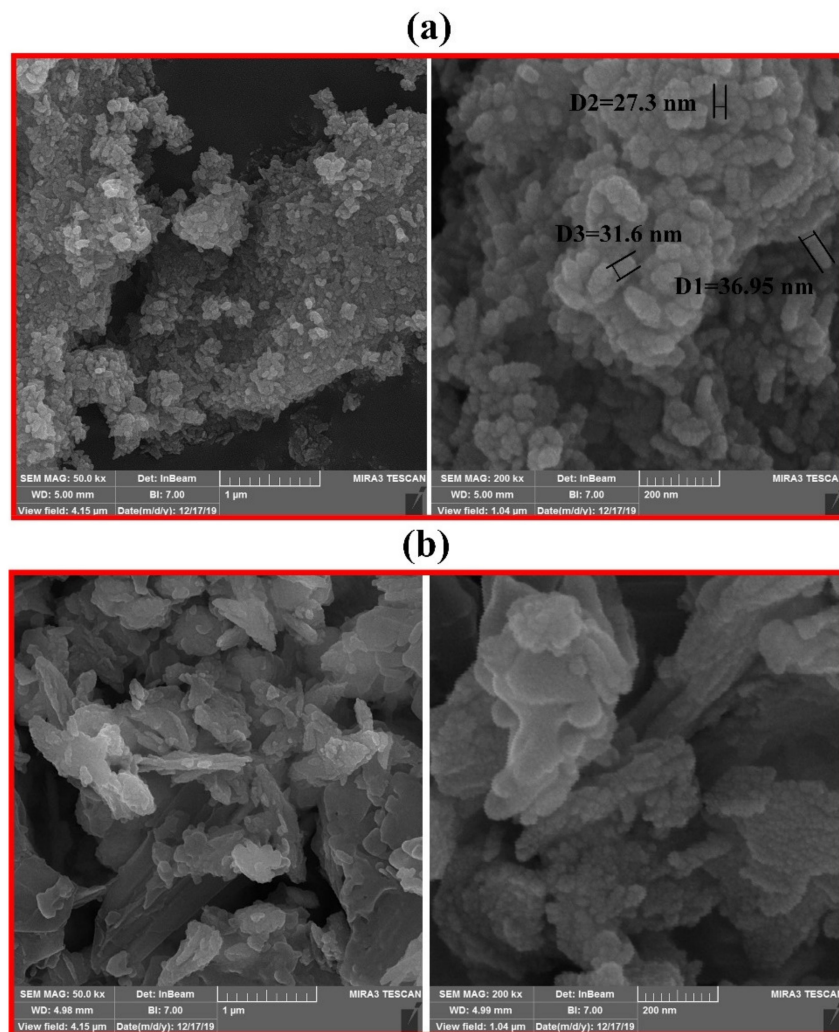


**Figure 2.** FESEM images of the samples: (a) CuO and (b) CuO-2.5G.

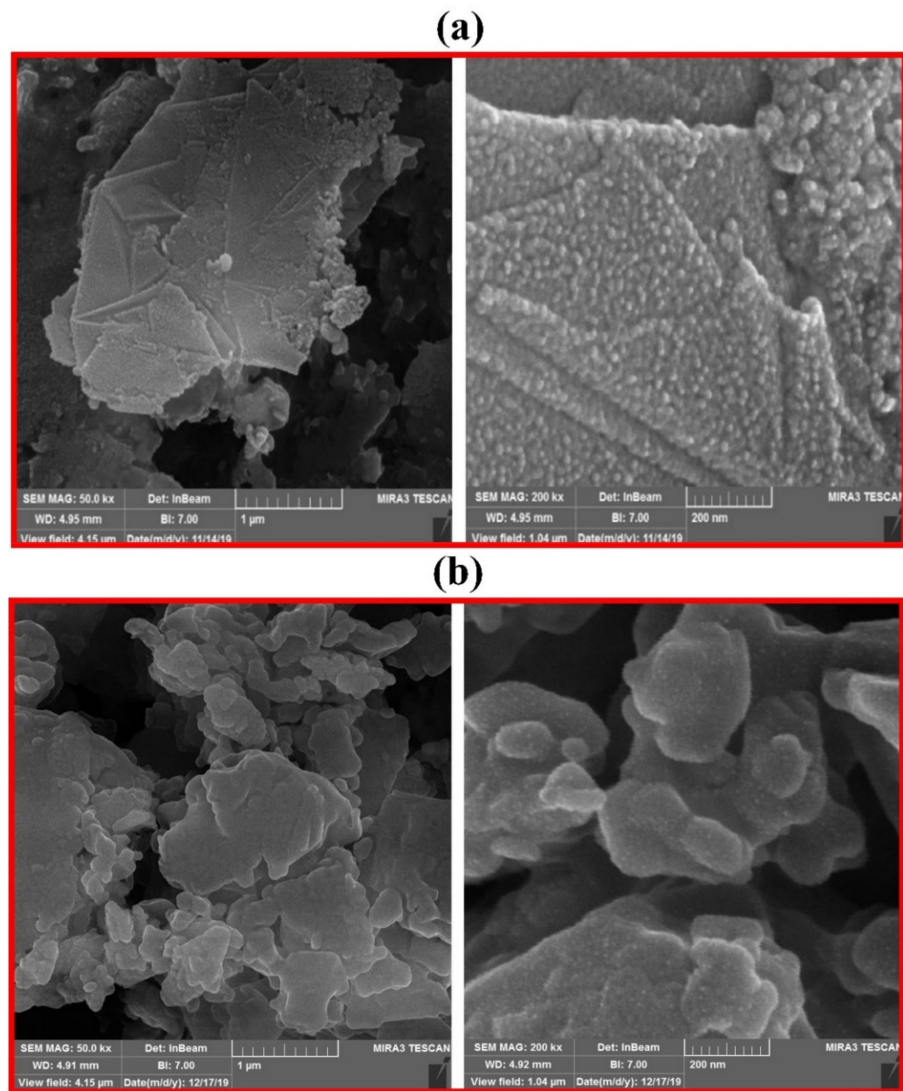


Figure 3. FESEM images of the samples: (a) CuO-5G and (b) CuO-10G.

Table 5. Weight percentage and atomic percentage of the elements present in the samples.

Sample	Element	Weight Percentage (%)	Atomic Percentage (%)	Error (%)
CuO	O	30.78	63.30	21.18
	Cu	69.22	36.70	1.04
CuO-2.5G	C	25.44	50.22	10.66
	O	17.39	27.58	10.66
	Cu	57.17	22.20	0.84
CuO-5G	C	59.06	76.20	13.94
	O	18.52	19.02	13.94
	Cu	22.42	4.78	0.73
CuO-10G	C	47.22	62.27	14.14
	O	33.66	33.15	14.14
	Cu	19.12	4.58	0.60

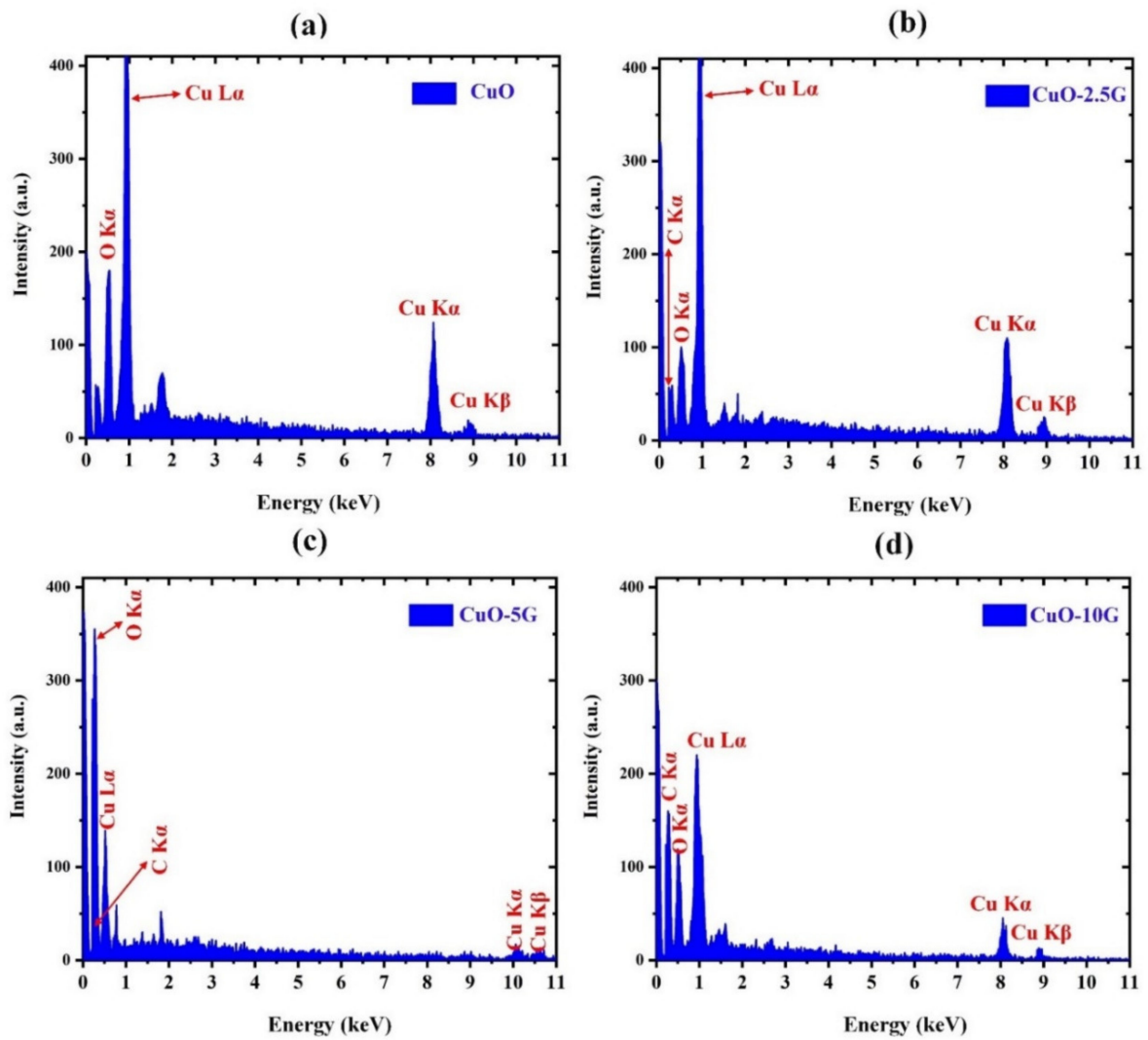


Figure 4. EDX spectra of the samples: (a) CuO, (b) CuO-2.5G, (c) CuO-5G and (d) CuO-10G.

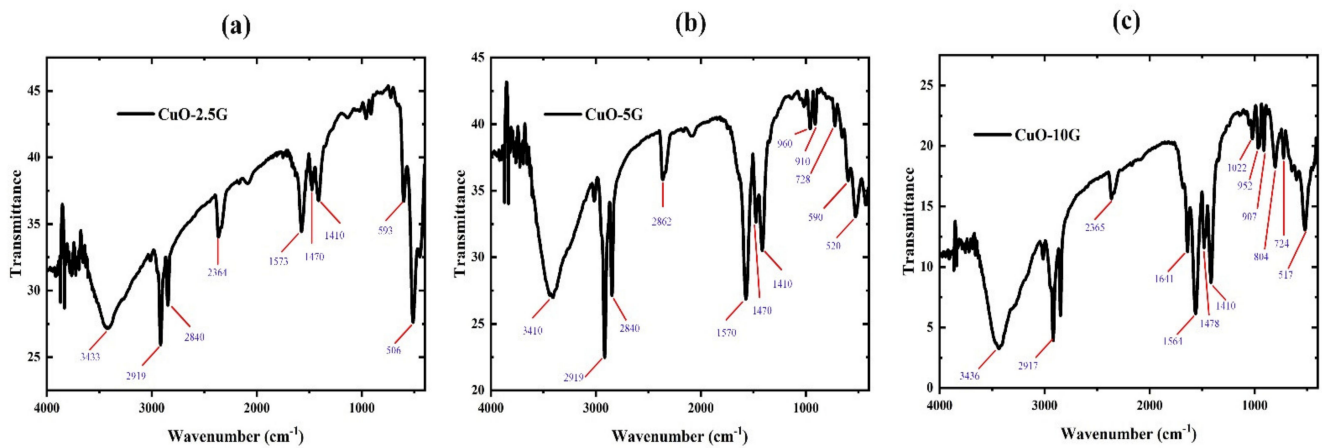


Figure 5. FTIR spectra of the samples: (a) CuO-2.5G, (b) CuO-5G, and (c) CuO-10G.



**Table 6.** Bond assignments of CuO-2.5G, CuO-5G and CuO-10G nanocomposites in FTIR spectra.

CuO-10G			CuO-5G			CuO-2.5G		
Reference	Vibraton Mode	k (cm <sup>-1</sup> )	Reference	Vibraton Mode	k (cm <sup>-1</sup> )	Reference	Vibraton Mode	k (cm <sup>-1</sup> )
[75]	Cu–O	517	[75]	Cu-O	520	[75]	Cu–O	506
[76]	C=O	724	[76]	Cu-O	590	[76]	Cu–O	593
[77]	C–C	804	[77]	C=O	728	[78]	C=O	1410
[75]	C=O	907	[75]	C=O	910	[78]	C=O	1470
[76]	C=O	952	[76]	C=O	960	[79]	C–O	1573
[78]	C–O–C	1022	[78]	C=O	1410	[78]	C=O	2364
[78]	C=O	1410	[78]	C=O	1470	[80]	C=O	2840
[79]	C=O	1478	[79]	C–O	1570	[80]	C–H	2919
[78]	C–O	1564	[78]	C=H	2862	[80]	O–H	3433
[80]	O–H	1641	[80]	C–H	2840	-	-	-
[80]	C=O	2365	[80]	C–H	2919	-	-	-
[80]	C–H	2917	[80]	O–H	3410	-	-	-
[80]	O–H	3436	-	-	-	-	-	-

### 3.3. Evaluation of Optical Bandgap

One of the most suitable tools for studying the band structure and bandgap energy of crystalline/non-crystalline systems is the analysis of optical absorption spectrum, especially the absorption edge in the ultraviolet and visible regions. Figure 6 shows the UV–visible absorption spectra of the pristine CuO and CuO-xG nanocomposites. As can be seen, the addition of graphene into CuO increases the absorption in the visible range and causes a red shift of the absorption edge toward higher wavelengths. Wider absorption spectrum directly increases charge generation efficiency and ultimately increases dye degradation [81,82]. To estimate the allowed direct optical bandgap energy, Tauc's plots are presented in Figure 7 for all prepared samples. Tauc's relation is expressed below [83].

$$(\alpha h\nu)^n = A(h\nu - E_g) \quad (2)$$

where A is a constant,  $h\nu$  is incident photon energy,  $E_g = hc/\lambda$  represents the optical bandgap energy,  $\alpha$  indicates the absorption coefficient, and n is an integer that determines the type of direct/indirect bandgap allowed or forbidden transitions and takes the value 2 for direct bandgap materials like CuO in our case. Extrapolating the linear part of the curve to the horizontal axis yields the optical bandgap energy (see Figure 7). The values obtained for  $E_g$  are given in Table 7. For pristine CuO, we found an optical bandgap of ~1.41 eV, which is close to the reported value. However, the incorporation of CuO with graphene reduces the bandgap value to around 1.29 eV. Additionally, increasing the amount of graphene from 2.5 to 5 and then 10 mg lowers the optical bandgap to 1.20 and 1.17 eV, respectively. The narrowed optical bandgap energy may occur due to the existence of defects in the intergranular regions and the introduction of energy levels between the conduction and the valence bands of CuO, mainly arising due to the chemical interaction of graphene and CuO [77].

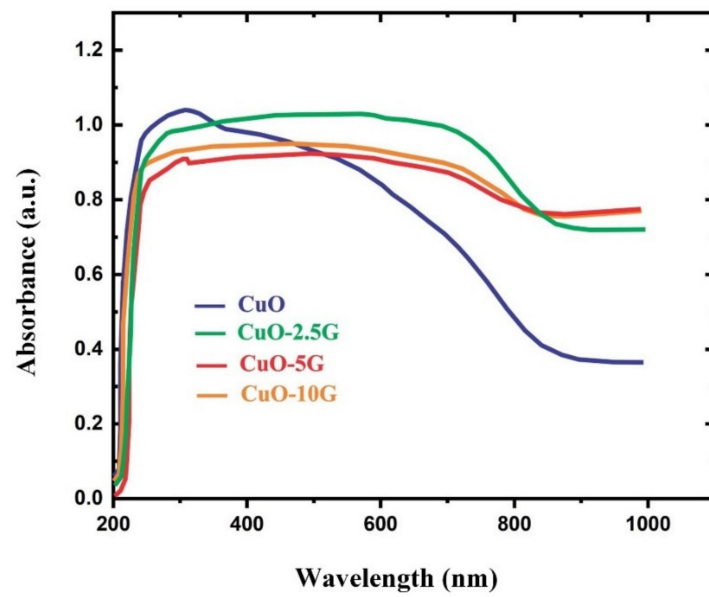


Figure 6. UV-Vis absorption spectra of the samples.

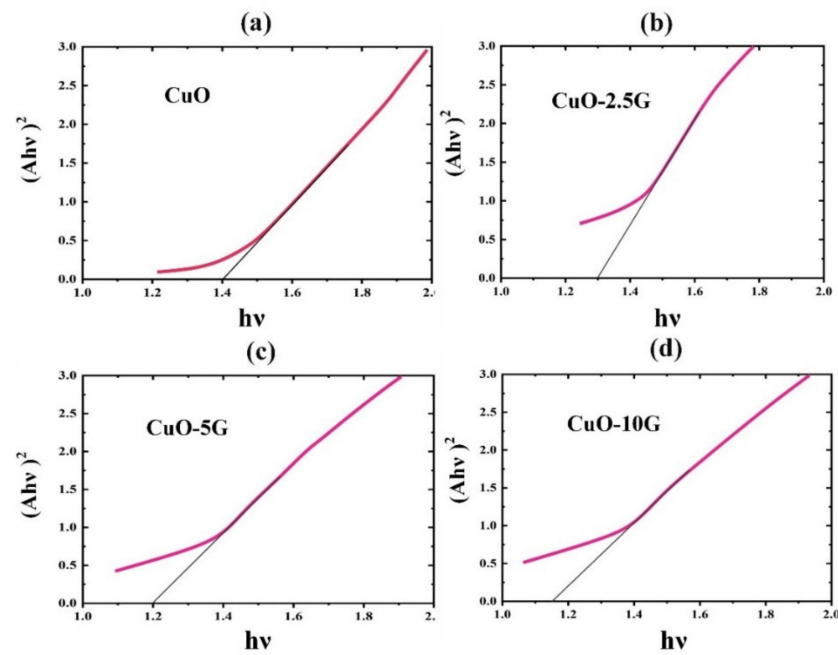


Figure 7. Tauc's plots of the samples: (a) CuO, (b) CuO-2.5G, (c) CuO-5G, (d) CuO-10G.

Table 7. Calculated optical bandgap energies for the synthesized samples.

Sample	Optical Bandgap Energy ( $\pm 0.01$ eV)
CuO	1.41
CuO-2.5G	1.29
CuO-5G	1.20
CuO-10G	1.17

### 3.4. Study of Photocatalytic Activity

Figure 8 shows the UV–visible absorption spectra of MB solution recorded at 1-h intervals during the photodegradation experiments of pristine CuO and CuO-xG ( $x = 2.5, 5$  and  $10$  mg) samples. It can be seen that MB exhibits a maximum absorption peak at

~664 nm. As is clear, the absorbance of MB in the presence of the samples decreased with increasing time of light irradiation. The photodegradation efficiency was determined for all samples by using the equation shown below [84]:

$$\text{Photodegradation efficiency (\%)} = [(A_0 - A_t)/A_0] \times 100\% = [(C_0 - C_t)/C_0] \times 100\% \quad (3)$$

where  $C_0$  is the initial concentration of MB,  $C_t$  is the concentration of MB at time  $t$ ,  $A_0$  is the initial absorbance of MB, and  $A_t$  is the absorbance after time  $t$  photo irradiation, recorded at the maximum absorbance wavelength for the MB. Figure 9a represents the photodegradation efficiency (%) of the sample in terms of time of light irradiation. The uncertainty in the photodegradation efficiencies is about 1%. Additionally, Figure 9b shows the rate of MB dye photodegradation by the synthesized samples. As can be seen from Figure 9a, after 9 h of irradiation, the photodegradation efficiencies of pristine CuO and CuO-2.5G, CuO-5G and CuO-10G samples are about 28%, 48%, 56% and 12%, respectively. The addition of graphene improved the photodegradation efficiency of CuO after 3 h of light irradiation (from ~9% to ~19%). From Figure 9a, increasing the amount of graphene from 2.5 to 5 mg increased the photodegradation efficiency again. Graphene has been reported to be a highly efficient absorbent for MB molecules [85,86]. Graphene acts as a substrate for copper oxide and hinders electron-hole recombination by trapping the charge carriers that have reached the semiconductor surface, resulting in an increase in the photodegradation efficiency. The graphene/GO sheet induces strong  $\pi_i-\pi_i$  conjugation with the molecules of MB [86,87]. There is electron transfer from the CuO to MB molecules when the energy matches or exceeds the band gaps of CuO the electrons are excited from the valence to conduction bands, and holes are generated. The photoelectrons are transferred to graphene. The conjugated graphene then transfers the electrons towards the MB molecules absorbed on the surface, causing the decomposition reaction. The concentration of MB molecules on surface of nanocomposites (CuO-xG) is greater than the CuO because of greater absorbing capacity of graphene which leads to the greater photocatalytic activity [33]. In addition to this, the presences of surface hydroxyl (eOH) groups causes trapping of holes to produce radicals which are excellent oxidizing agents for organic pollutants in water [88]. On the basis of EDX and XRD data, it is confirmed that CuO and CuO-xG have high amounts of Cu-eOH, which can provide sources of OH radicals and facilitates the decomposition of MB. However, further increasing the amount of graphene from 5 to 10 mg surprisingly reduced the photodegradation efficiency. Finally, it can be concluded that CuO-5G nanocomposite has the best photocatalytic activity among the prepared samples. The lower catalytic activity of CuO-10G than CuO nanoparticles can be explained by the particles size. It has been reported that activity of any material is related to its size [89]. The smaller the size of the nanoparticles, the lower the rate of electron-hole recombination. The order of average grain diameter of synthesize material is CuO-5G (20.11 nm) < CuO-2.5G (28.92 nm) < CuO (31.95 nm) < CuO-10G (40.85 nm). The particle size of CuO is smaller than the CuO-10G as confirmed by the XRD and SEM, so it has a higher photocatalytic activity than CuO-10G.

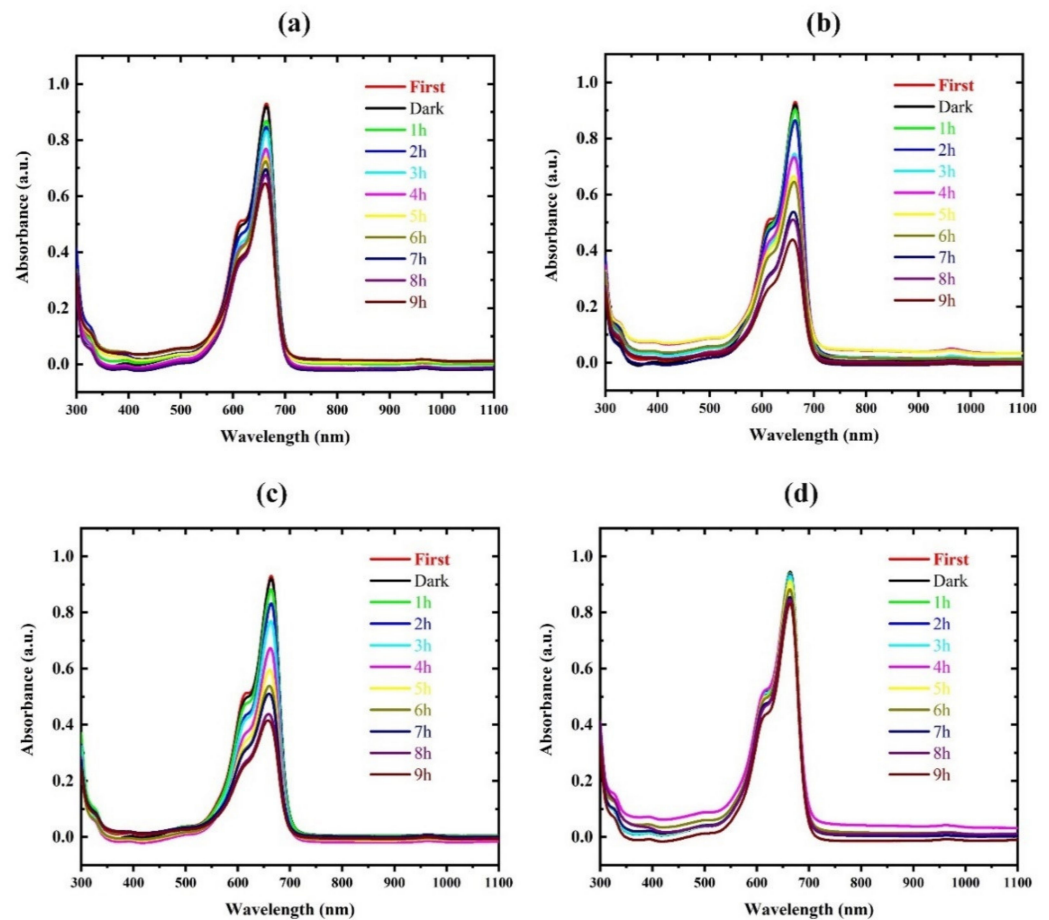


Figure 8. Time-dependent absorption spectra of MB solution during light irradiation in the presence of: (a) pristine CuO, (b) CuO-2.5G, (c) CuO-5G, and (d) CuO-10G.

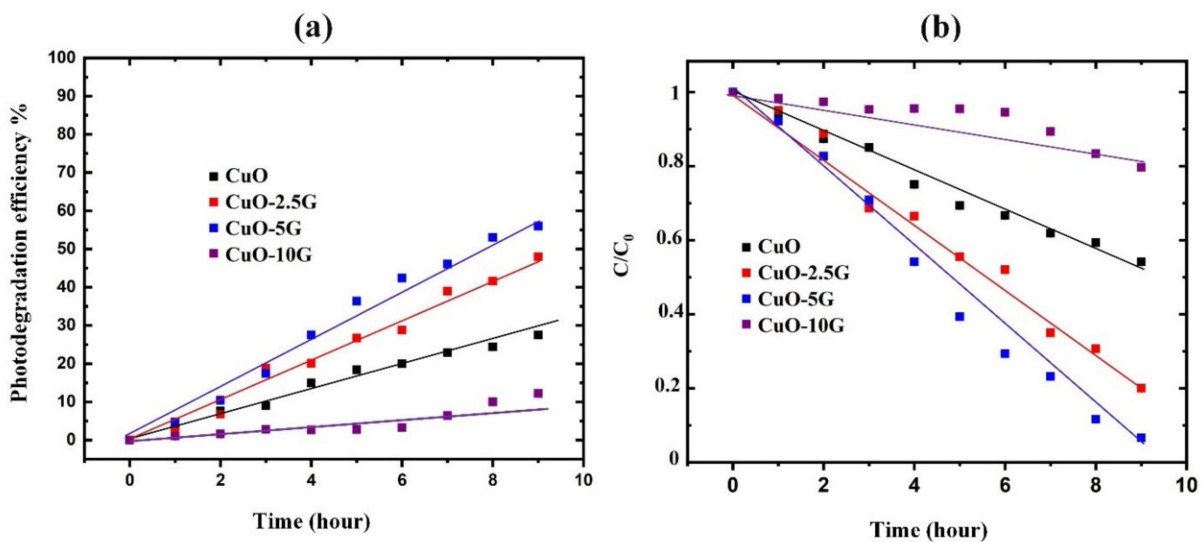


Figure 9. (a) Photodegradation efficiency (%) of pristine CuO, CuO-2.5G, CuO-5G and CuO-10G nanocomposites in terms of time of light irradiation and (b) the rate of MB dye photodegradation by the samples.

#### 4. Conclusions

Pristine CuO and CuO-xG (2.5, 5, and 10 mg) nanocomposites were successfully synthesized by a simple hydrothermal method and tested and tested by XRD, FESEM, EDX, FTIR and UV-Vis techniques. XRD studies showed that with increasing the amount of

graphene incorporated with CuO, the average crystallite size of graphene in the nanocomposite increases. The sample CuO-5G had the smallest average crystallite size of CuO (~10.19 nm) among the nanocomposites. FESEM images showed a grain structure for the pristine CuO sample with an average grain diameter of around 31.95 nm. The average diameters of grains grown on the graphene sheets were found to be around 28.92, 20.11 and 40.85 nm for CuO-2.5G, CuO-5G and CuO-10G samples, respectively. FTIR studies exhibited the absorption peaks related to the main covalent bonds present in the structure of the samples. It was found that the optical bandgap energy decreases with increasing the amount of graphene in the nanocomposite; it decreased from 1.41 eV in pristine CuO sample to 1.17 eV in the CuO-10G sample. The potential of the nanocomposites as a photocatalyst was evaluated by photodegradation of methylene blue dye under visible light irradiation. After 9 h of irradiation, the photodegradation efficiencies of pristine CuO, CuO-2.5G, CuO-5G and CuO-10G samples were about 28%, 48%, 56% and 12%, respectively. In fact, graphene acts as a substrate for copper oxide and hinders electron-hole recombination by trapping the charge carriers that have reached the semiconductor surface, resulting in an increase in the photodegradation efficiency.

**Author Contributions:** Conceptualization, I.R. and A.A.; methodology, A.F.A.; software, D.B.; validation, E.R.A. and R.L.; resources, M.A.; data curation, M.J.; writing—original draft preparation, A.A.; writing—review and editing, R.L. project administration, M.A.; funding acquisition, M.J. All authors have read and agreed to the published version of the manuscript.

**Funding:** The authors would like to acknowledge the support of the deputy for research and innovation-Ministry of education, Kingdom of Saudi Arabia for this research through grant (NU/IFC/INT/01/003) under the institutional funding committee at Najran University Kingdom of Saudi Arabia.

**Institutional Review Board Statement:** Not applicable.

**Informed Consent Statement:** Not applicable.

**Data Availability Statement:** Not applicable.

**Conflicts of Interest:** The authors declare no conflict of interest.

## References

1. Upadhyay, R.K.; Soin, N.; Roy, S.S. Role of graphene/metal oxide composites as photocatalysts, adsorbents and disinfectants in water treatment: A review. *RSC Adv.* **2014**, *4*, 3823–3851. [[CrossRef](#)]
2. Quan, Q.; Lin, X.; Zhang, N.; Xu, Y.-J. Graphene and its derivatives as versatile templates for materials synthesis and functional applications. *Nanoscale* **2017**, *9*, 2398–2416. [[CrossRef](#)]
3. Huang, W.-Y.; Wang, G.-Q.; Li, W.-H.; Li, T.-T.; Ji, G.-J.; Ren, S.-C.; Jiang, M.; Yan, L.; Tang, H.-T.; Pan, Y.-M.; et al. Porous ligand creates new reaction route: Bifunctional single-atom palladium catalyst for selective distannylation of terminal alkynes. *Chem* **2020**, *6*, 2300–2313. [[CrossRef](#)]
4. Ahmad, A.; Jini, D.; Aravind, M.; Parvathiraja, C.; Ali, R.; Kiyani, M.Z.; Allothman, A. A novel study on synthesis of egg shell based activated carbon for degradation of methylene blue via photocatalysis. *Arab. J. Chem.* **2020**, *13*, 8717–8722. [[CrossRef](#)]
5. Aravind, M.; Ahmad, A.; Ahmad, I.; Amalanathan, M.; Naseem, K.; Mary, S.M.M.; Parvathiraja, C.; Hussain, S.; Algarni, T.S.; Pervaiz, M. Critical green routing synthesis of silver nps using jasmine flower extract for biological activities and photocatalytic degradation of methylene blue. *J. Environ. Chem. Eng.* **2021**, *9*, 104877. [[CrossRef](#)]
6. Pervaiz, M.; Ahmad, I.; Yousaf, M.; Kirn, S.; Munawar, A.; Saeed, Z.; Adnan, A.; Gulzar, T.; Kamal, T.; Ahmad, A. Synthesis, spectral and antimicrobial studies of amino acid derivative schiff base metal (Co, Mn, Cu, and Cd) complexes. *Spectrochim. Acta Part A Mol. Biomol. Spectrosc.* **2019**, *206*, 642–649. [[CrossRef](#)]
7. Hussain, S.; Khan, A.J.; Arshad, M.; Javed, M.S.; Ahmad, A.; Shah, S.S.A.; Khan, M.R.; Akram, S.; Ali, S.; AlOthman, Z.A. Charge storage in binder-free 2D-hexagonal CoMoO<sub>4</sub> nanosheets as a redox active material for pseudocapacitors. *Ceram. Int.* **2021**, *47*, 8659–8667. [[CrossRef](#)]
8. Zhan, M.; Hussain, S.; AlGarni, T.S.; Shah, S.; Liu, J.; Zhang, X.; Ahmad, A.; Javed, M.S.; Qiao, G.; Liu, G. Facet controlled polyhedral ZIF-8 MOF nanostructures for excellent NO<sub>2</sub> gas-sensing applications. *Mater. Res. Bull.* **2021**, *136*, 111133. [[CrossRef](#)]
9. Kashif, M.; Ngaini, Z.; Harry, A.V.; Vekariya, R.L.; Ahmad, A.; Zuo, Z.; Sahari, S.K.; Hussain, S.; Khan, Z.A.; Alarifi, A. An experimental and dft study on novel dyes incorporated with natural dyes on titanium dioxide (TiO<sub>2</sub>) towards solar cell application. *Appl. Phys. A* **2020**, *126*, 1–13. [[CrossRef](#)]



10. Saleem, M.; Irfan, M.; Tabassum, S.; Albaqami, M.D.; Javed, M.S.; Hussain, S.; Pervaiz, M.; Ahmad, I.; Ahmad, A.; Zuber, M. Experimental and theoretical study of highly porous lignocellulose assisted metal oxide photoelectrodes for dye-sensitized solar cells. *Arab. J. Chem.* **2021**, *14*, 102937. [[CrossRef](#)]
11. Kashif, M.; Jaafar, E.; Bhadja, P.; Low, F.W.; Sahari, S.K.; Hussain, S.; Loong, F.K.; Ahmad, A.; AlGarni, T.S.; Shafa, M. Effect of potassium permanganate on morphological, structural and electro-optical properties of graphene oxide thin films. *Arab. J. Chem.* **2021**, *14*, 102953. [[CrossRef](#)]
12. Zhang, X.Z.; Xu, P.H.; Liu, G.W.; Ahmad, A.; Chen, X.H.; Zhu, Y.L.; Alothman, A.; Hussain, S.; Qiao, G.J. Synthesis, characterization and wettability of cu-sn alloy on the si-implanted 6h-sic. *Coatings* **2020**, *10*, 906. [[CrossRef](#)]
13. Fallah, Z.; Zare, E.N.; Ghomi, M.; Ahmadijokani, F.; Amini, M.; Tajbakhsh, M.; Arjmand, M.; Sharma, G.; Ali, H.; Ahmad, A. Toxicity and remediation of pharmaceuticals and pesticides using metal oxides and carbon nanomaterials. *Chemosphere* **2021**, *275*, 130055. [[CrossRef](#)] [[PubMed](#)]
14. Bibi, S.; Ahmad, A.; Anjum, M.A.R.; Haleem, A.; Siddiq, M.; Shah, S.S.; Al Kahtani, A. Photocatalytic degradation of malachite green and methylene blue over reduced graphene oxide (rgo) based metal oxides (rgo-Fe<sub>3</sub>O<sub>4</sub>/TiO<sub>2</sub>) nanocomposite under uv-visible light irradiation. *J. Environ. Chem. Eng.* **2021**, *9*, 105580. [[CrossRef](#)]
15. Ahmad, I.; Jamal, M.A.; Iftikhar, M.; Ahmad, A.; Hussain, S.; Asghar, H.; Saeed, M.; Yousaf, A.B.; Karri, R.R.; Al-kadhi, N.S. Lanthanum-zinc binary oxide nanocomposite with promising heterogeneous catalysis performance for the active conversion of 4-nitrophenol into 4-aminophenol. *Coatings* **2021**, *11*, 537. [[CrossRef](#)]
16. Javed, M.S.; Khan, A.J.; Ahmad, A.; Siyal, S.H.; Akram, S.; Zhao, G.; Bahajaj, A.A.A.; Ouladsmame, M.; Alfakeer, M. Design and fabrication of bimetallic oxide nanonest-like structure/carbon cloth composite electrode for supercapacitors. *Ceram. Int.* **2021**, *47*, 30747–30755. [[CrossRef](#)]
17. Javed, M.S.; Najim, T.; Hussain, I.; Batool, S.; Idrees, M.; Mehmood, A.; Imran, M.; Assiri, M.A.; Ahmad, A.; Shah, S.S.A. 2D V<sub>2</sub>O<sub>5</sub> ultrathin nanoflakes as a binder-free electrode material for high-performance pseudocapacitor. *Ceram. Int.* **2021**, *47*, 25152–25157. [[CrossRef](#)]
18. Beena, V.; Rayar, S.; Ajitha, S.; Ahmad, A.; Albaqami, M.D.; Alsabar, F.A.A.; Sillanpää, M. Synthesis and characterization of sr-doped znse nanoparticles for catalytic and biological activities. *Water* **2021**, *13*, 2189. [[CrossRef](#)]
19. Siyal, S.H.; Javed, M.S.; Ahmad, A.; Sajjad, M.; Batool, S.; Khan, A.J.; Akram, S.; Alothman, A.A.; Alshgari, R.A.; Najam, T. Free-standing 3D Co<sub>3</sub>O<sub>4</sub>@ nf micro-flowers composed of porous ultra-long nanowires as an advanced cathode material for supercapacitor. *Curr. Appl. Phys.* **2021**, *31*, 221–227. [[CrossRef](#)]
20. Syah, R.; Ahmad, A.; Davarpanah, A.; Elveny, M.; Ramdan, D.; Albaqami, M.D.; Ouladsmame, M. Incorporation of Bi<sub>2</sub>O<sub>3</sub> residuals with metallic Bi as high performance electrocatalyst toward hydrogen evolution reaction. *Catalysts* **2021**, *11*, 1099. [[CrossRef](#)]
21. Abbas, Q.; Javed, M.S.; Ahmad, A.; Siyal, S.H.; Asim, I.; Luque, R.; Albaqami, M.D.; Tighezza, A.M. ZnO nano-flowers assembled on carbon fiber textile for high-performance supercapacitor's electrode. *Coatings* **2021**, *11*, 1337. [[CrossRef](#)]
22. Bibi, S.; Khan, A.; Khan, S.; Ahmad, A.; Sakhawat Shah, S.; Siddiq, M.; Iqbal, A.; Al-Kahtani, A.A. Synthesis of cr doped limnpo<sub>4</sub> cathode materials and investigation of their dielectric properties. *Int. J. Energy Res.* **2021**, *2021*, 1–12.
23. Raees, A.; Jamal, M.; Ahmad, A.; Ahmad, I.; Saeed, M.; Habila, M.; AlMasoud, N.; Alomar, T. Synthesis and characterization of ceria incorporated nickel oxide nanocomposite for promising degradation of methylene blue via photocatalysis. *Int. J. Environ. Sci. Technol.* **2021**, 1–8. [[CrossRef](#)]
24. Beena, V.; Rayar, S.; Ajitha, S.; Ahmad, A.; Iftikhar, F.J.; Abualnaja, K.M.; Alomar, T.S.; Ouladsmame, M.; Ali, S. Photocatalytic dye degradation and biological activities of cu-doped znse nanoparticles and their insights. *Water* **2021**, *13*, 2561. [[CrossRef](#)]
25. Meyer, B.K.; Polity, A.; Reppin, D.; Becker, M.; Hering, P.; Klar, P.J.; Sander, T.; Reindl, C.; Benz, J.; Eickhoff, M.; et al. Binary copper oxide semiconductors: From materials towards devices. *Phys. Status Solidi (B)* **2012**, *249*, 1487–1509. [[CrossRef](#)]
26. Masudy-Panah, S.; Kakran, M.; Lim, Y.-F.; Chua, C.S.; Tan, H.R.; Dalapati, G.K. Graphene nanoparticle incorporated CuO thin film for solar cell application. *J. Renew. Sustain. Energy* **2016**, *8*, 43507. [[CrossRef](#)]
27. Chen, X.; Wang, D.; Wang, T.; Yang, Z.; Zou, X.; Wang, P.; Luo, W.; Li, Q.; Liao, L.; Hu, W.; et al. Enhanced photoresponsivity of a GaAs nanowire metal-semiconductor-metal photodetector by adjusting the fermi level. *ACS Appl. Mater. Interfaces* **2019**, *11*, 33188–33193. [[CrossRef](#)] [[PubMed](#)]
28. Tian, Y.; Liu, Y.; Wang, W.-P.; Zhang, X.; Peng, W. CuO nanoparticles on sulfur-doped graphene for nonenzymatic glucose sensing. *Electrochim. Acta* **2015**, *156*, 244–251. [[CrossRef](#)]
29. Li, Y.; Macdonald, D.D.; Yang, J.; Qiu, J.; Wang, S. Point defect model for the corrosion of steels in supercritical water: Part I, film growth kinetics. *Corros. Sci.* **2020**, *163*, 108280. [[CrossRef](#)]
30. Kim, D.S.; Lee, G.H.; Lee, S.; Kim, J.C.; Lee, H.J.; Kim, B.K.; Kim, D.W. Electrocatalytic performance of CuO/graphene nanocomposites for Li–O<sub>2</sub> batteries. *J. Alloys Compd.* **2017**, *707*, 275–280. [[CrossRef](#)]
31. Ji, B.; Zhang, F.; Song, X.; Tang, Y. A novel potassium-ion-based dual-ion battery. *Adv. Mater.* **2017**, *29*, 1700519. [[CrossRef](#)] [[PubMed](#)]
32. Choi, J.; Oh, H.; Han, S.-W.; Ahn, S.; Noh, J.; Park, J.B. Preparation and characterization of graphene oxide supported Cu, Cu<sub>2</sub>O, and CuO nanocomposites and their high photocatalytic activity for organic dye molecule. *Curr. Appl. Phys.* **2017**, *17*, 137–145. [[CrossRef](#)]

33. Pandiyarajan, T.; Saravanan, R.; Karthikeyan, B.; Gracia, F.; Mansilla, H.D.; Gracia-Pinilla, M.A.; Mangalaraja, R.V. Sonochemical synthesis of CuO nanostructures and their morphology dependent optical and visible light driven photocatalytic properties. *J. Mater. Sci. Mater. Electron.* **2017**, *28*, 2448–2457. [[CrossRef](#)]
34. Sharma, A.; Dutta, R.K. Studies on the drastic improvement of photocatalytic degradation of acid orange-74 dye by TPPO capped CuO nanoparticles in tandem with suitable electron capturing agents. *RSC Adv.* **2015**, *5*, 43815–43823. [[CrossRef](#)]
35. Bhattacharjee, A.; Ahmaruzzaman, M. CuO nanostructures: Facile synthesis and applications for enhanced photodegradation of organic compounds and reduction of p-nitrophenol from aqueous phase. *RSC Adv.* **2016**, *6*, 41348–41363. [[CrossRef](#)]
36. Liu, R.; Yin, J.; Du, W.; Gao, F.; Fan, Y.; Lu, Q. Monodisperse CuO hard and hollow nanospheres as visible-light photocatalysts. *Eur. J. Inorg. Chem.* **2013**, *2013*, 1358–1362. [[CrossRef](#)]
37. Arshad, A.; Iqbal, J.; Siddiq, M.; Ali, M.U.; Ali, A.; Shabbir, H.; Nazeer, U.B.; Saleem, M.S. Solar light triggered catalytic performance of graphene-CuO nanocomposite for waste water treatment. *Ceram. Int.* **2017**, *43*, 10654–10660. [[CrossRef](#)]
38. Park, K.-W.; Sung, Y.-E.; Han, S.; Yun, Y.; Hyeon, T. Origin of the enhanced catalytic activity of carbon nanocoil-supported PtRu alloy electrocatalysts. *J. Phys. Chem. B* **2004**, *108*, 939–944. [[CrossRef](#)]
39. Li, X.; Shi, T.; Li, B.; Chen, X.; Zhang, C.; Guo, Z.; Zhang, Q. Subtractive manufacturing of stable hierarchical micro-nano structures on AA5052 sheet with enhanced water repellence and durable corrosion resistance. *Mater. Des.* **2019**, *183*, 108152. [[CrossRef](#)]
40. Cheng, J.-Z.; Tan, Z.-R.; Xing, Y.-Q.; Shen, Z.-Q.; Zhang, Y.-J.; Liu, L.-L.; Yang, K.; Chen, L.; Liu, S.-Y. Exfoliated conjugated porous polymer nanosheets for highly efficient photocatalytic hydrogen evolution. *J. Mater. Chem. A* **2021**, *9*, 5787–5795. [[CrossRef](#)]
41. Liu, H.; Li, X.X.; Liu, X.Y.; Ma, Z.H.; Yin, Z.Y.; Yang, W.W.; Yu, Y.S. Schiff-base-rich gC<sub>x</sub>N<sub>4</sub> supported PdAg nanowires as an efficient Mott–Schottky catalyst boosting photocatalytic dehydrogenation of formic acid. *Rare Met.* **2021**, *40*, 808–816. [[CrossRef](#)]
42. Allen, M.J.; Tung, V.; Kaner, R.B. Honeycomb Carbon: A review of graphene. *Chem. Rev.* **2010**, *110*, 132–145. [[CrossRef](#)]
43. Rao, C.N.R.; Sood, A.K.; Subrahmanyam, K.S.; Govindaraj, A. Graphene: The new two-dimensional nanomaterial. *Angew. Chem. Int. Ed.* **2009**, *48*, 7752–7777. [[CrossRef](#)] [[PubMed](#)]
44. Park, S.; Ruoff, R.S. Chemical methods for the production of graphenes. *Nat. Nanotechnol.* **2009**, *4*, 217–224. [[CrossRef](#)]
45. Schwierz, F. Graphene transistors. *Nat. Nanotechnol.* **2010**, *5*, 487–496. [[CrossRef](#)]
46. Wang, D.; Choi, D.; Li, J.; Yang, Z.; Nie, Z.; Kou, R.; Hu, D.; Wang, C.; Saraf, L.V.; Zhang, J.; et al. Self-Assembled TiO<sub>2</sub>–Graphene hybrid nanostructures for enhanced Li-ion insertion. *ACS Nano* **2009**, *3*, 907–914. [[CrossRef](#)]
47. Sheng, M.; Zhang, F.; Ji, B.; Tong, X.; Tang, Y. A novel tin-graphite dual-ion battery based on sodium-ion electrolyte with high energy density. *Adv. Energy Mater.* **2017**, *7*, 1601963. [[CrossRef](#)]
48. Yoo, E.; Okata, T.; Akita, T.; Kohyama, M.; Nakamura, J.; Honma, I. Enhanced electrocatalytic activity of Pt subnanoclusters on graphene nanosheet surface. *Nano Lett.* **2009**, *9*, 2255–2259. [[CrossRef](#)]
49. Wang, X.; Zhi, L.; Tsao, H.N.; Tomović, Ž.; Li, J.; Müllen, K. Transparent carbon films as electrodes in organic solar cells. *Angew. Chem. Int. Ed.* **2008**, *47*, 2990–2992. [[CrossRef](#)] [[PubMed](#)]
50. Li, G.; Xu, C. Hydrothermal synthesis of 3D Ni<sub>x</sub>Co<sub>1-x</sub>S<sub>2</sub> particles/graphene composite hydrogels for high performance supercapacitors. *Carbon* **2015**, *90*, 44–52. [[CrossRef](#)]
51. Lu, C.H.; Yang, H.H.; Zhu, C.L.; Chen, X.; Chen, G.N. A graphene platform for sensing biomolecules. *Angew. Chem.* **2009**, *121*, 4879–4881. [[CrossRef](#)]
52. Wang, H.; Robinson, J.T.; Diankov, G.; Dai, H. Nanocrystal growth on graphene with various degrees of oxidation. *J. Am. Chem. Soc.* **2010**, *132*, 3270–3271. [[CrossRef](#)]
53. Lv, B.-J.; Wang, S.; Xu, T.-W.; Guo, F. Effects of minor Nd and Er additions on the precipitation evolution and dynamic recrystallization behavior of Mg–6.0Zn–0.5Mn alloy. *J. Magnes. Alloy.* **2020**, *9*, 840–852. [[CrossRef](#)]
54. Li, X.; Sheng, X.; Guo, Y.; Lu, X.; Wu, H.; Chen, Y.; Zhang, L.; Gu, J. Multifunctional HDPE/CNTs/PW composite phase change materials with excellent thermal and electrical conductivities. *J. Mater. Sci. Technol.* **2021**, *86*, 171–179. [[CrossRef](#)]
55. Babushkina, E.A.; Belokopytova, L.V.; Grachev, A.M.; Meko, D.; Vaganov, E.A. Variation of the hydrological regime of Bele-Shira closed basin in Southern Siberia and its reflection in the radial growth of *Larix sibirica*. *Reg. Environ. Chang.* **2017**, *17*, 1725–1737. [[CrossRef](#)]
56. Anwar, A.W.; Majeed, A.; Iqbal, N.; Ullah, W.; Shuaib, A.; Ilyas, U.; Bibi, F.; Rafique, H.M. Specific capacitance and cyclic stability of graphene based metal/metal oxide nanocomposites: A review. *J. Mater. Sci. Technol.* **2015**, *31*, 699–707. [[CrossRef](#)]
57. Liang, Y.; Li, Y.; Wang, H.; Zhou, J.; Wang, J.; Regier, T.; Dai, H. Co<sub>3</sub>O<sub>4</sub> nanocrystals on graphene as a synergistic catalyst for oxygen reduction reaction. *Nat. Mater.* **2011**, *10*, 780–786. [[CrossRef](#)]
58. Chen, S.; Brown, L.; Levendorf, M.; Cai, W.; Ju, S.-Y.; Edgeworth, J.; Li, X.; Magnuson, C.W.; Velamakanni, A.; Piner, R.D.; et al. Oxidation resistance of graphene-coated Cu and Cu/Ni alloy. *ACS Nano* **2011**, *5*, 1321–1327. [[CrossRef](#)]
59. Goli, P.; Ning, H.; Li, X.; Lu, C.Y.; Novoselov, K.S.; Balandin, A.A. Thermal properties of graphene–copper–graphene heterogeneous films. *Nano Lett.* **2014**, *14*, 1497–1503. [[CrossRef](#)]
60. Udayabhaskar, R.; Mangalaraja, R.; Sahlevani, S.F.; Perarasu, V.; Karthikeyan, B.; Contreras, D.; Gracia-Pinilla, M. Graphene induced band gap widening and luminescence quenching in ceria:graphene nanocomposites. *J. Alloys Compd.* **2019**, *770*, 1221–1228. [[CrossRef](#)]
61. Lu, Z.-Q.; Zhao, L.; Ding, H.; Chen, L.-Q. A dual-functional metamaterial for integrated vibration isolation and energy harvesting. *J. Sound Vib.* **2021**, *509*, 116251. [[CrossRef](#)]

62. Zhu, H.; An, Y.; Shi, M.; Li, Z.; Chen, N.; Yang, C.; Xiao, P. Porous N-doped carbon/MnO<sub>2</sub> nanoneedles for high performance ionic liquid-based supercapacitors. *Mater. Lett.* **2021**, *296*, 129837. [[CrossRef](#)]
63. Suresh, R.; Udayabhaskar, R.; Sandoval, C.; Ramírez, E.; Mangalaraja, R.V.; Mansilla, H.D.; Contreras, D.; Yáñez, J. Effect of reduced graphene oxide on the structural, optical, adsorption and photocatalytic properties of iron oxide nanoparticles. *New J. Chem.* **2018**, *42*, 8485–8493. [[CrossRef](#)]
64. Tian, Y.; Lin, L.; Chen, S.; Zhu, S.; Zhang, H.; Yu, W.; Ning, H.; Hu, N. Defects engineering of Fe<sub>2</sub>O<sub>3</sub>@Sn<sub>2</sub>O<sub>3</sub> nanosheet arrays for high-performance hybrid supercapacitor. *J. Energy Storage* **2021**, *42*, 103123. [[CrossRef](#)]
65. Aadil, M.; Shaheen, W.; Warsi, M.F.; Shahid, M.; Khan, M.A.; Ali, Z.; Haider, S.; Shakir, I. Superior electrochemical activity of  $\alpha$ -Fe<sub>2</sub>O<sub>3</sub>/rGO nanocomposite for advance energy storage devices. *J. Alloys Compd.* **2016**, *689*, 648–654. [[CrossRef](#)]
66. Mohan, B.S.; Ravi, K.; Anjaneyulu, R.B.; Sree, G.S.; Basavaiah, K. Fe<sub>2</sub>O<sub>3</sub>/RGO nanocomposite photocatalyst: Effective degradation of 4-Nitrophenol. *Phys. B Condens. Matter* **2019**, *553*, 190194. [[CrossRef](#)]
67. Wang, B.; Wu, X.-L.; Shu, C.-Y.; Guo, Y.-G.; Wang, C.-R. Synthesis of CuO/graphene nanocomposite as a high-performance anode material for lithium-ion batteries. *J. Mater. Chem.* **2010**, *20*, 10661–10664. [[CrossRef](#)]
68. Liu, Y.; Sun, M.; Yuan, Y.; Wu, Q.; Wang, H.; He, Y.; Lin, Z.; Zhou, F.; Ling, M.; Qian, C.; et al. Accommodation of silicon in an interconnected copper network for robust Li-ion storage. *Adv. Funct. Mater.* **2020**, *30*, 1910249. [[CrossRef](#)]
69. Zhang, H.; Lin, L.; Wu, B.; Hu, N. Vertical carbon skeleton introduced three-dimensional MnO<sub>2</sub> nanostructured composite electrodes for high-performance asymmetric supercapacitors. *J. Power Sources* **2020**, *476*, 228527. [[CrossRef](#)]
70. Chen, Y.; Chen, K.; Bai, H.; Li, L. Electrochemically reduced graphene porous material as light absorber for light-driven thermoelectric generator. *J. Mater. Chem.* **2012**, *22*, 17800–17804. [[CrossRef](#)]
71. Ghijsen, J.; Tjeng, L.H.; van Elp, J.; Eskes, H.; Westerink, J.; Sawatzky, G.A.; Czyzyk, M.T. Electronic structure of Cu<sub>2</sub>O and CuO. *Phys. Rev. B* **1988**, *38*, 11322–11330. [[CrossRef](#)]
72. Wang, J.; Li, F.; Xu, M. Synthesis and Characterization of Nanoscale CuO Powders. In Proceedings of the 55th International Convention of Society of Wood Science and Technology, Beijing, China, 27–31 August 2012.
73. Sarkar, C.; Dolui, S.K. Synthesis of copper oxide/reduced graphene oxide nanocomposite and its enhanced catalytic activity towards reduction of 4-nitrophenol. *RSC Adv.* **2015**, *5*, 60763–60769. [[CrossRef](#)]
74. Yusoff, N. Synthesis of Functionalized Graphene/Copper Oxide (CuO) Nanocomposites and Their Catalytic Activity/NORAZRIENA Binti Yusoff. Ph.D. Thesis, University of Malaya, Lumpur, Malaya, 2013.
75. Erdoğan, İ.Y.; Güllü, Ö. Optical and structural properties of CuO nanofilm: Its diode application. *J. Alloys Compd.* **2010**, *492*, 378–383. [[CrossRef](#)]
76. Jadhav, M.S.; Kulkarni, S.; Raikar, P.; Barretto, D.A.; Vootla, S.K.; Raikar, U.S. Green biosynthesis of CuO & Ag–CuO nanoparticles from *Malus domestica* leaf extract and evaluation of antibacterial, antioxidant and DNA cleavage activities. *New J. Chem.* **2018**, *42*, 204–213. [[CrossRef](#)]
77. El-Trass, A.; ElShamy, H.; El-Mehasseb, I.; El-Kemary, M. CuO nanoparticles: Synthesis, characterization, optical properties and interaction with amino acids. *Appl. Surf. Sci.* **2012**, *258*, 2997–3001. [[CrossRef](#)]
78. Muhamad, E.N.; Irmawati, R.; Abdullah, A.H.; Taufiq-Yap, Y.H.; Hamid, S.A. Effect of number of washing on the characteristics of copper oxide nanopowders. *Malays. J. Anal. Sci.* **2007**, *11*, 294–301.
79. Sabeeh, S.H.; Hussein, H.A.; Judran, H.K. Synthesis of a complex nanostructure of CuO via a coupled chemical route. *Mater. Res. Express* **2016**, *3*, 125025. [[CrossRef](#)]
80. Zhang, Y.; Tang, Z.-R.; Fu, X.; Xu, Y.-J. TiO<sub>2</sub>–graphene nanocomposites for gas-phase photocatalytic degradation of volatile aromatic pollutant: Is TiO<sub>2</sub>–graphene truly different from other TiO<sub>2</sub>–carbon composite materials? *ACS Nano* **2010**, *4*, 7303–7314. [[CrossRef](#)]
81. Sakthivel, S.; Kisch, H. Daylight photocatalysis by carbon-modified titanium dioxide. *Angew. Chem. Int. Ed.* **2003**, *42*, 4908–4911. [[CrossRef](#)]
82. Manickathai, K.; Viswanathan, S.K.; Alagar, M. Synthesis and characterization of CdO and CdS nanoparticles. *IJPAP* **2008**, *46*, 561–564.
83. Pouredal, H.; Kadkhodaie, A. Synthetic CeO<sub>2</sub> nanoparticle catalysis of methylene blue photodegradation: Kinetics and mechanism. *Chin. J. Catal.* **2010**, *31*, 1328–1334. [[CrossRef](#)]
84. Ramesha, G.; Kumara, A.V.; Muralidhara, H.; Sampath, S. Graphene and graphene oxide as effective adsorbents toward anionic and cationic dyes. *J. Colloid Interface Sci.* **2011**, *361*, 270–277. [[CrossRef](#)]
85. Yang, S.-T.; Chen, S.; Chang, Y.; Cao, A.; Liu, Y.; Wang, H. Removal of methylene blue from aqueous solution by graphene oxide. *J. Colloid Interface Sci.* **2011**, *359*, 24–29. [[CrossRef](#)] [[PubMed](#)]
86. Liu, T.; Li, Y.; Du, Q.; Sun, J.; Jiao, Y.; Yang, G.; Wang, Z.; Xia, Y.; Zhang, W.; Wang, K.; et al. Adsorption of methylene blue from aqueous solution by graphene. *Colloids Surf. B Biointerfaces* **2012**, *90*, 197–203. [[CrossRef](#)]
87. Akhavan, O.; Azimirad, R.; Safa, S.; Hasani, E. CuO/Cu(OH)<sub>2</sub> hierarchical nanostructures as bactericidal photocatalysts. *J. Mater. Chem.* **2011**, *21*, 9634–9640. [[CrossRef](#)]
88. Li, Y.; Yang, X.-Y.; Rooke, J.; Van Tendeloo, G.; Su, B.-L. Ultralong Cu(OH)<sub>2</sub> and CuO nanowire bundles: PEG200-directed crystal growth for enhanced photocatalytic performance. *J. Colloid Interface Sci.* **2010**, *348*, 303–312. [[CrossRef](#)]
89. Hagfeldt, A.; Graetzel, M. Light-induced redox reactions in nanocrystalline systems. *Chem. Rev.* **1995**, *95*, 49–68. [[CrossRef](#)]